AGU PUBLICATIONS

JGR

Journal of Geophysical Research: Atmospheres

RESEARCH ARTICLE
10.1002/2017JD027107

Key Points:
- Relationship between ULF waves and polar cap atmospheric conditions
- Solar wind influence on high-latitude atmosphere
- ULF waves modulation of the microphysical processes in the clouds

Correspondence to:
M. Regi,
mauro.regi@aquila.infn.it

Citation:
Regi, M., G. Redaelli, P. Franci, and M. De Lauretis (2017), ULF geomagnetic activity effects on tropospheric temperature, specific humidity, and cloud cover in Antarctica, during 2003–2010, *J. Geophys. Res. Atmos.*, *122*, doi:10.1002/2017JD027107.

Received 10 MAY 2017
Accepted 10 JUN 2017
Accepted article online 21 JUN 2017

ULF geomagnetic activity effects on tropospheric temperature, specific humidity, and cloud cover in Antarctica, during 2003–2010

Mauro Regi[1], Gianluca Redaelli[2], Patrizia Francia[1], and Marcello De Lauretis[1]

[1]Department of Physical and Chemical Sciences, University of L'Aquila, L'Aquila, Italy, [2]CETEMPS/Department of Physical and Chemical Sciences, University of L'Aquila, L'Aquila, Italy

Abstract In the present study we investigated the possible relationship between the ULF geomagnetic activity and the variations of several atmospheric parameters. In particular, we compared the ULF activity in the Pc1-2 frequency band (100 mHz–5 Hz), computed from geomagnetic field measurements at Terra Nova Bay in Antarctica, with the tropospheric temperature T, specific humidity Q, and cloud cover (high cloud cover, medium cloud cover, and low cloud cover) obtained from reanalysis data set. The statistical analysis was conducted during the years 2003–2010, using correlation and Superposed Epoch Analysis approaches. The results show that the atmospheric parameters significantly change following the increase of geomagnetic activity within 2 days. These changes are evident in particular when the interplanetary magnetic field B_z component is oriented southward ($B_z < 0$) and the B_y component duskward ($B_y > 0$). We suggest that both the precipitation of electrons induced by Pc1-2 activity and the intensification of the polar cap potential difference, modulating the microphysical processes in the clouds, can affect the atmosphere conditions.

1. Introduction

The terrestrial atmosphere essentially manifests its dynamics through its interaction with Sun's radiation energy. An additional source of energy comes from the solar wind (SW). In particular, SW energy can be partially converted in magnetohydrodynamic ultralow frequency fluctuations (ULF, 1 mHz–5 Hz), which propagate inside the magnetosphere, and can lead to diffusion and precipitation of relativistic electrons (>100 keV) from the radiation belts [*Regi et al.*, 2015; *Mann et al.*, 2004; *Blum et al.*, 2015; *Rodger et al.*, 2008], with potential effects on the atmospheric dynamics (see *Mironova et al.* [2015] and *Lam and Tinsley* [2016] for a review).

In particular, the electron precipitation seems to play an important role, by ionization, on the atmospheric chemical composition [*Rozanov et al.*, 2005; *Lu et al.*, 2008; *Seppälä et al.*, 2009, 2013; *Baumgaertner et al.*, 2011] and conductivity variations [*Tinsley and Zhou*, 2006; *Tinsley et al.*, 2007]. Energetic particle precipitation occurs after pitch angle scattering, due to gyroresonant interaction with electromagnetic ion cyclotron (EMIC) waves, in the ULF Pc1-2 (100 mHz–5 Hz) frequency range [*Engebretson et al.*, 2008]. EMIC waves are generated at the magnetic equator by unstable distributions of ring current ions during geomagnetic storms [*Arnoldy et al.*, 2005] and can be observed on the ground, also at high latitudes, after propagation as Alfvén (shear) waves along the ambient magnetic field lines [*Mursula et al.*, 1994; *Dyrud et al.*, 1997]. They can be regarded as a proxy of the particle precipitation. Moreover, the ULF activity in general is associated to storms and substorms, i.e., to the occurrence of a southward interplanetary magnetic field (IMF) and, at high latitudes, to a polar cap electric field; therefore, it can be regarded also as a proxy of the polar cap potential difference [*Yagova et al.*, 2002; *Francia et al.*, 2009; *Regi et al.*, 2016].

The whole process can modify the atmospheric current system in the Global Electric Circuit (GEC) model [*Tinsley and Zhou*, 2006], with a tropospheric response, due to production of space charge in clouds, affecting cloud microphysics and in turn the occurrence of cloud layers that may also change the radiative balance [*Regi et al.*, 2016; *Francia et al.*, 2015]. In particular, during highly perturbed geomagnetic conditions, the energy transferred to the Earth system could be significant, playing a role in controlling the atmospheric parameter variations [*Francia et al.*, 2015; *de Wit and Watermann*, 2010] and cloud processes, during which there is a

continuous conversion of energy between different forms (e.g., thermal energy to latent heat release). It is a matter of fact that water vapor converts into cloud via several mechanisms (see *Tinsley and Yu* [2004] and *Lam and Tinsley* [2016] for a review).

The accumulation of charge on droplets and aerosol particles, most importantly the interstitial cloud condensation nuclei (CCN) and ice-forming nuclei (IFN), directly affects scavenging rates of their collision with cloud droplets. Scavenging is due to collisions between the nuclei and droplets, entailing size-dependent collection of nuclei and changes in their size distribution and overall concentration. It affects a number of microphysical processes, which cause changes in macroscopic cloud properties and in turn partitioning of energy flow in the system. In particular, the charge can increase or decrease the scavenging rates, dependent on size, changing the concentrations and size distributions. Size distribution changes in CCN produce size distribution changes in droplets, affecting coagulation, precipitation, latent heat transfer, and cloud cover. Scavenging of ice-forming nuclei by supercooled droplets promotes contact ice nucleation, releasing latent heat. The latent heat changes cause storm invigoration [*Rosenfeld et al.*, 2008] and in winter storms can cause changes in the amplitude of Rossby waves and blocking. Since the typical lifetime of CCN in an air mass can be up to 10 days, the change in their properties can effect also later cycle of evaporation/condensation, flux of latent heat, and the amount of water vapor released into the troposphere.

In this work we investigated the possible relationship between the Pc1-2 fluctuations, possibly driven by the SW, and the variations of the atmospheric parameters, using both correlation and Superposed Epoch Analysis approaches.

We found that Pc1-2 power is clearly related with both temperature T and specific humidity Q ($Q = m_v/(m_v + m_d)$, where m_v and m_d are, respectively, the mass of water vapor and the mass of dry air in a certain volume of air [*Wallace and Hobbs*, 2011]), which can be considered a parameter related to water vapor, and with cloud cover CC (the percentage of the sky hidden by all visible clouds) at high (HCC, >6 km), medium (MCC, $3 < h < 6$ km), and low (LCC, 0–3 km) altitudes.

2. Materials and Methods

In this work we used search-coil magnetometer data, recorded at Terra Nova Bay (TNB, AACGM 80.01°S, 306.94°E) at a sampling rate of 1 s, during 2003–2010. We estimated the Pc1-2 geomagnetic total power P in the horizontal component, applying the Fourier transform to 1 h nonoverlapped time series. The Pc1-2 power was computed only between 100 and 500 mHz, due to the 1 s sampling rate. The power spectral densities are frequency smoothed, with a final frequency resolution of approximately 1.4 mHz, and converted into nT^2/Hz unit using the transfer function of the instrument (see *De Lauretis et al.* [2010] for more details). Then, we computed the daily median of P. Finally, following previous investigations [*Regi et al.*, 2016; *Francia et al.*, 2015], we used $\log_{10} P$ (hereafter $\hat{P}$) instead of P as an activity index of ULF waves, since P undergoes impulsive variations of several orders of magnitude, and thus, $\hat{P}$ is more suitable to be compared with atmospheric parameters; $\hat{P}$ follows an almost Gaussian distribution [*Regi et al.*, 2015] being easily comparable to the results of the Monte Carlo test, for which Gaussian white noise is used.

As parameters representative of atmospheric conditions, we used tropospheric temperature T, specific humidity Q, and the cloud cover CC from the Monitoring Atmospheric Composition and Climate (MACC) data set which is a global reanalysis data set of atmospheric composition data, produced by assimilating satellite data into a global model and data assimilation system [see *Inness et al.*, 2013, and references therein] as a function of time t, geographical latitudes λ, and longitudes ϕ, with resolutions, respectively, of 1 day and 1.125° lat/lon, and pressure levels p over 23 pressure levels (from 1000 to 1 hPa). In our work the altitudes are estimated from the pressure levels p by means of the relation $h = A \ln\left(p_0/p\right)$, where $A = 7.0$ km and $p_0 = 10^3$ hPa [see, e.g., *Regi et al.*, 2016], and we restricted the analysis to the tropospheric heights.

The ULF geomagnetic fluctuation power has a clearly detectable ~27 day periodicity (and its subharmonics) related with the Sun's synodic periodicity; signatures of such periodicities have been found also in the surface air temperature [*Francia et al.*, 2015] and in the temperature and zonal wind reanalysis data [*Regi et al.*, 2016], but the atmospheric parameters are strongly affected by several phenomena with different periodicities that can obscure weaker effects particularly during local summer months. On this regard, atmospheric parameters should be suitably filtered before any comparative analysis with solar wind and geomagnetic data and preferentially local winter months should be analyzed.

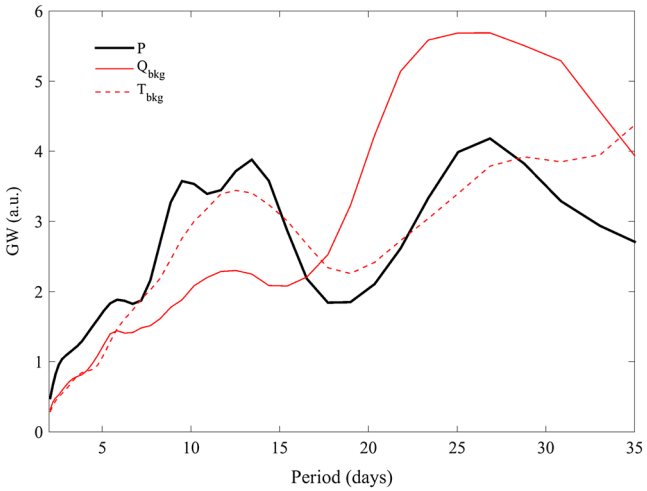

Figure 1. The comparison between the average GW power spectra of Pc1-2 (black), with the average background of temperature T_{bkg} and specific humidity Q_{bkg}, during winter months in the interval 2008–2010. Each spectrum is normalized to its total power.

In the present work we compared the ULF power and the tropospheric parameter variations using the Superposed Epoch Analysis (SEA) method, which is useful to evidence low-amplitude fluctuations embedded in a background signal [*Chree*, 1913; *Forbush et al.*, 1983], and the correlation/cross-correlation analysis. Both methods are described below.

(a) For SEA, we used the moving-average procedures as indicated by *Laken and Čalogović* [2013] in order to identify and remove from the original time series periodicities greater than ~54 days (i.e., 2 times the Sun's synodic periodicity).

Using $\hat{P}$ as key parameter, we defined, as key events, power peaks greater than −5 and higher than the seasonal trend (i.e., 54 days smoothed time series).

We defined the day corresponding to the power peak as epoch and considered a time window of 5 days, i.e., 2 days before and after the event. Only nonoverlapped time periods are taken into account in our investigations, so that we used a statistically independent data set; with this choice the number of case events is 54. Once the 5 day time series are selected, we computed the composite mean C and the related standard error of the mean (SEM) (see *Laken and Čalogović* [2013] for details). SEA analyses are also supported by Monte Carlo test in order to highlight statistically significant correspondence between input and output variations; we used 10,000 Gaussian white noise series with an amplitude of 0.5 times the actual standard deviation of the examined time series.

(b) The correlation analysis was performed between input and output parameters. Before the correlation analysis, the original daily geomagnetic and atmospheric time series were band-pass filtered in the range 20–30 days. After the analysis, we estimated the 90% confidence level obtained by means of a Monte Carlo test over 10,000 Gaussian white noise series, filtered by the same procedure of the real data.

Solar wind, interplanetary magnetic field, and geomagnetic activity *AE* index hourly values, provided by OMNIweb (http://cdaweb.gsfc.nasa.gov), are also examined.

3. Statistical Results

In the present work we compared time series during local winter months in the years 2003–2010 (except 2005, when there are long data gaps), using reanalysis data in the 80–90°S geographic latitude range and 0–10 km altitude range, since we are interested in the phenomena occurring in the troposphere (i.e., below ~10 km). The SEA is performed on the zonal means of the examined atmospheric parameters (i.e., using longitudinally averaged data), as a function of altitude and latitude. Regarding the correlation analysis, we examined all time series at each point in the troposphere. The experimental results are discussed in the following sections.

3.1. Signatures of Sun's Synodic Periodicity in the Assimilated Data Set

In order to investigate the spectral correspondence between $\hat{P}$ (input) and tropospheric T and Q (outputs) parameters, we performed a wavelet analysis of the high-pass filtered time series, obtained by removing the 54 days moving average from the original data. T and Q were taken in the latitude range 80–90°S and at all tropospheric heights. We used Morlet wavelet with dimensionless frequency $\omega_0 \approx 6$, in order to obtain a wavelet scale almost identical to the Fourier periodicity [*Torrence and Compo*, 1998], consistent with *Regi et al.* [2016].

For each year we computed the global wavelet (GW) power spectrum in the periodicity range 2–40 days of P, T, and Q, where the GW of Q and T was height averaged, resulting functions of latitude and longitude. As outlined in the section 1, the tropospheric dynamics is affected by several physical mechanisms, which makes

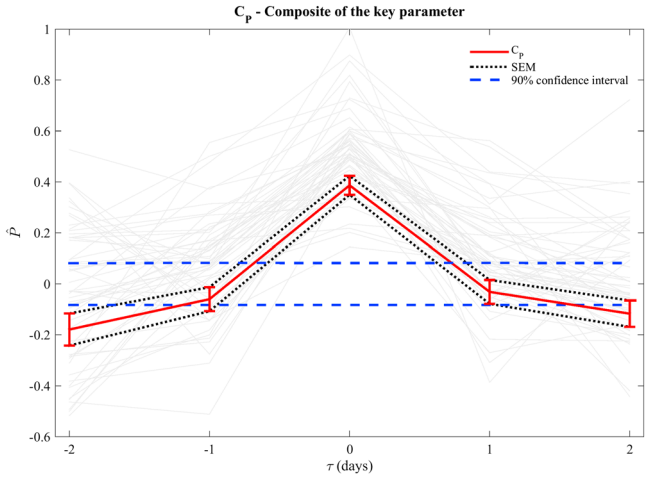

Figure 2. The composite of key parameter C_P (red) of selected 54 stochastically independent events, each one of 5 days duration (gray lines), together with SEM (red error bars and dashed black lines) and the 90% confidence intervals (blue dashed lines) evaluated by means of a Monte Carlo test.

it difficult to identify a geomagnetic activity signature in the GW of atmospheric parameters. Therefore, we compared the spectrum of Pc1-2 activity with the background spectra of Q and T [*Vellante et al.*, 1989]

Each background spectra is evaluated by means of an iterative and convergent procedure in which, at any step, the median GW power spectrum was recomputed removing all single spectra with enhancements of power, at any period, whose ratio with the current median GW was greater than a given ratio R_{GW}. We are confident that this procedure yields background spectra which are representative of the persistent features in the examined parameter. For a value of $R_{GW} = 1.5$ the spectra concurring to the background spectrum are between 10% and 50% of the original spectra depending on the year and parameter. This procedure yields background spectra, for each year, that are representative of the local persistent activity of the parameters under analysis. It was applied to the years 2008–2010 when solar activity was at its minimum and ULF power fluctuations was characterized by stable ~27 days periodicity.

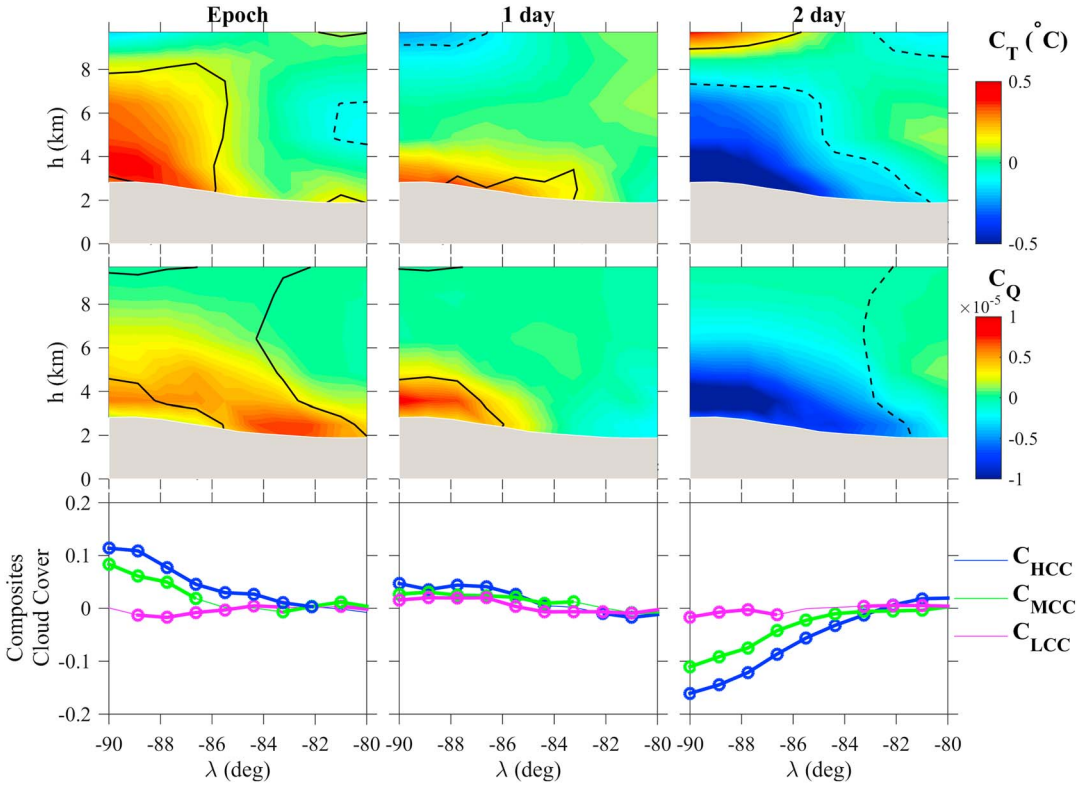

Figure 3. (top and middle rows) Composites of the zonal mean of temperature C_T (°C) and specific humidity C_Q of the 54 selected epochs, together with the 90% confidence levels (solid and dashed lines); also shown is the longitudinally averaged Antarctic profile (gray region). (bottom row) Composite mean of cloud cover C_{LCC} (<3 km), C_{MCC} ($3 < h < 6$ km), and C_{HCC} (>6 km): the bold lines mark composites statistically relevant.

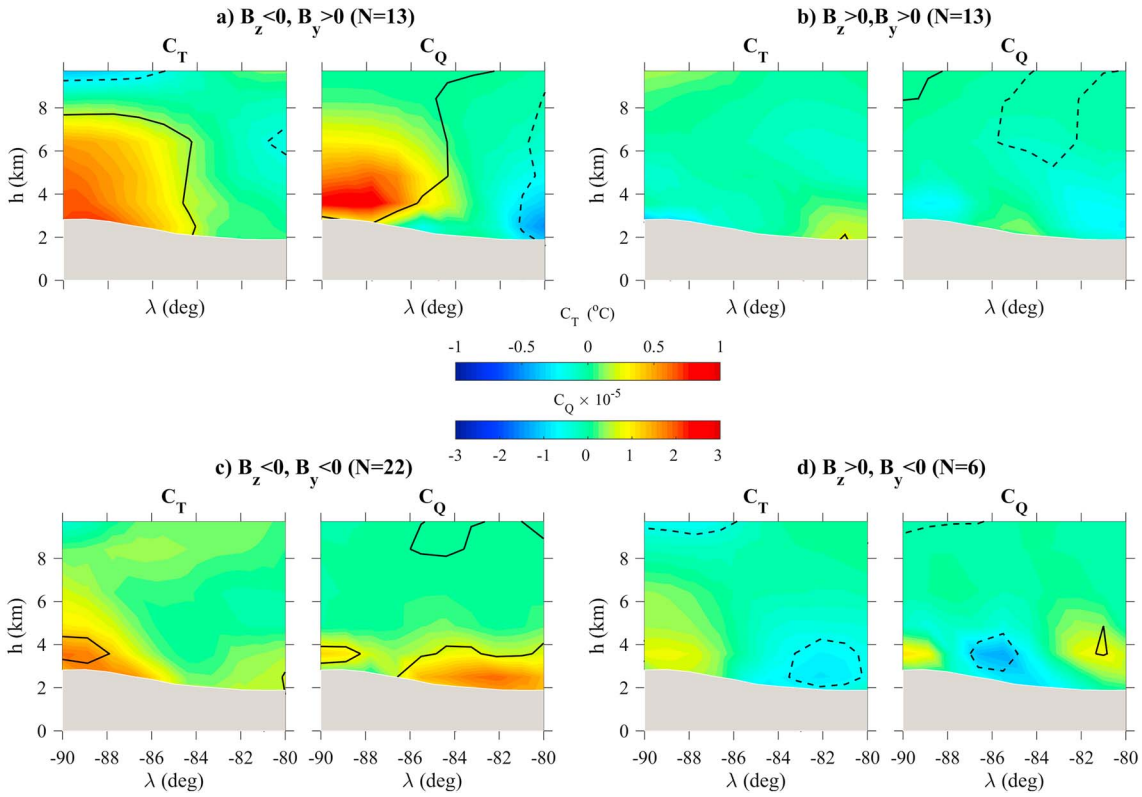

Figure 4. Composite mean at the epoch ($\tau = 0$) of temperature C_T and specific humidity C_Q with the Monte Carlo test (90% contour levels), for different interplanetary magnetic field conditions. For each couple of panels, *N* indicates the number of selected cases. In each panel, the longitudinally averaged Antarctic profile is also shown (gray region).

Figure 1 shows the 3 year average of the GW of *P* and the averaged background spectra Q_{bkg} and T_{bkg}. In order to compare the spectral trends on the same scale, the spectra are normalized to their total power.

It can be seen that a remarkable correspondence exists between Pc1-2 and tropospheric parameters around the ~27 day periodicity (more clear with Q_{bkg}) and around its first and second subharmonics (i.e., 13.5 and 9 days), confirming the correspondence between Pc1-2 and atmospheric parameters found in previous investigations [*Francia et al.*, 2015; *Regi et al.*, 2016].

3.2. Superposed Epoch Analysis With Monte Carlo Test

Figure 2 shows the composite mean of ULF power C_P (key parameter), resulting from SEA analysis, over winter months during 2003–2010 years (54 nonoverlapping subintervals). It can be seen that C_P (red line) clearly shows a power peak at the epoch, well outside the 90% confidence intervals (magenta lines), within 1 day.

The SEA was applied to tropospheric data series, obtaining composites of temperature C_T and specific humidity C_Q at different heights and latitudes at the epoch and 1–2 days after, as shown in Figure 3. We can see that both C_T and C_Q show significant positive values up to 1 day after the epoch, at deep polar latitudes (80–90°S) below the tropopause ($h < 8$ km).

These results suggests that, probably, Pc1-2 power affects the specific humidity and the tropospheric temperature within 1–2 days. The results are also consistent with *Francia et al.* [2015] who found significant correlation between surface air temperature at TNB ~1 day after ULF power fluctuations and with *Troshichev and Janzhura* [2004] who observed a temperature response within 1 day in the Antarctic plateau, during disturbed geomagnetic periods at tropospheric heights. Conversely, 2 days after the epoch, C_T and C_Q reach negative values.

As outlined in section 1, the atmospheric charge can increase or decrease the scavenging rates, changing the concentrations and size distributions of CCN and IFN, in turn modulating the resulting droplet concentrations

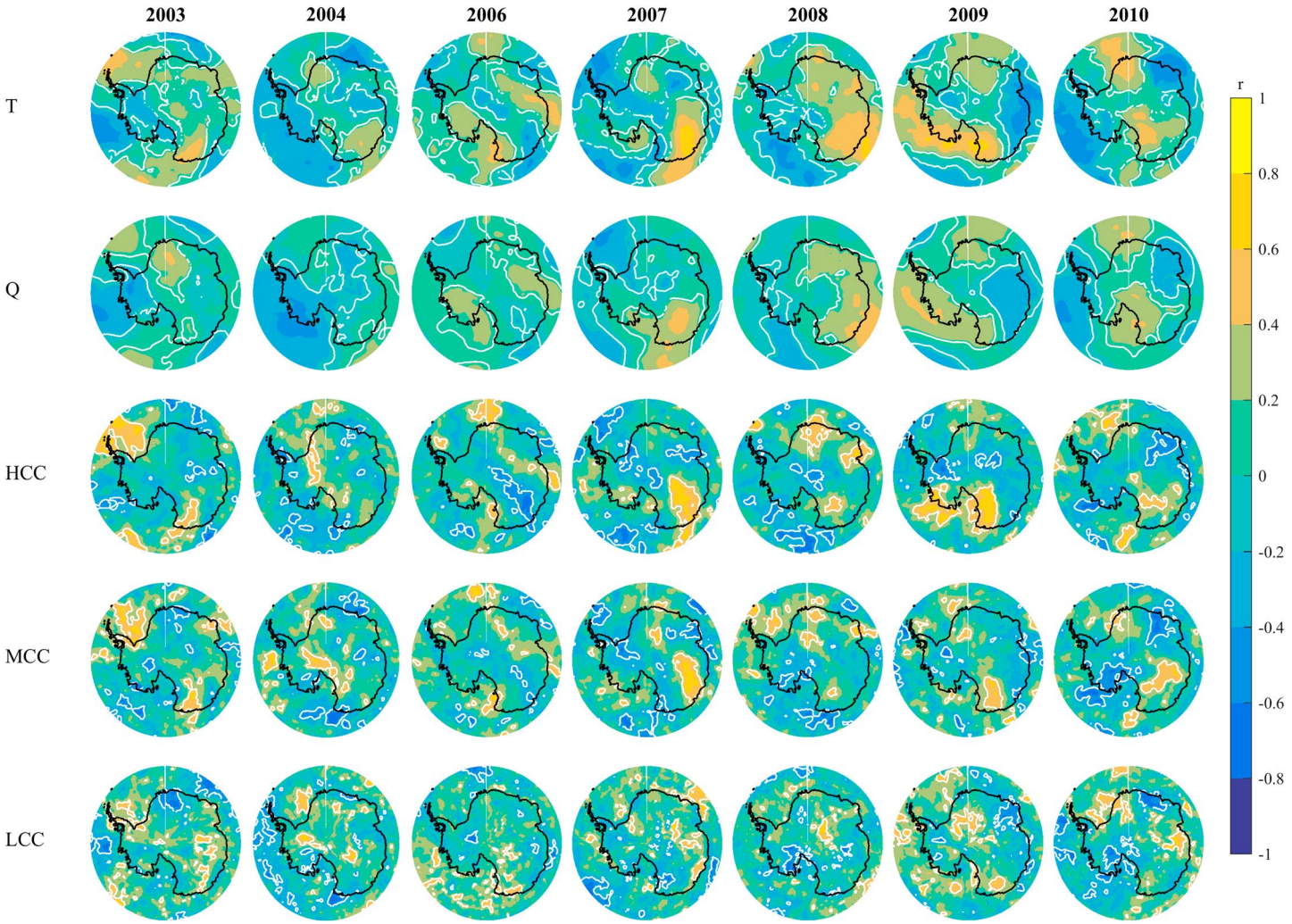

Figure 5. (first to fifth panels) Correlation coefficient maps between $\hat{P}$ with T, Q (height averaged), HCC, MCC, and LCC during 2003–2010. In each panel, the white contour lines mark the 90% confidence levels, estimated by means of a Monte Carlo test. The geographic latitude range is 60–90°S.

and size distributions and can affect ice production, the amount of water vapor released in the atmosphere, and the cloud cover. These changes would then lead to a change in the partitioning of atmospheric energy and modulate the amount of latent heat released in the process.

We examined the cloud cover (zonal mean) composite averages computed on low, medium, and high cloud cover composite mean that we indicated as C_{LCC}, C_{MCC}, and C_{HCC}, respectively (see Figure 3, bottom row). It can be seen that the main effect consists in an increase in the high and medium cloud covers at the epoch and 1 day after (blue and green lines) and a decrease 2 days after the epoch.

More clear results are attained by taking into account the interplanetary magnetic field direction, in particular the B_y and B_z components that are related with polar cap electrodynamic activity: B_z is important in the reconnection process in the dayside magnetopause, while B_y affects the latitudinal dawn-dusk electrostatic potential asymmetry [*Tinsley and Heelis*, 1993].

Figure 4 shows the composite mean of T and Q corresponding to different interplanetary magnetic field directions. It can be clearly observed that a strong increase of both composites occurs during $B_z < 0$ conditions. Regarding C_T, high values are observed for B_z <0 and B_y >0 (top left), at the highest latitudes in the polar cap. Similar results are observed during B_z <0 and B_y <0 conditions, perhaps confined to lower tropospheric heights.

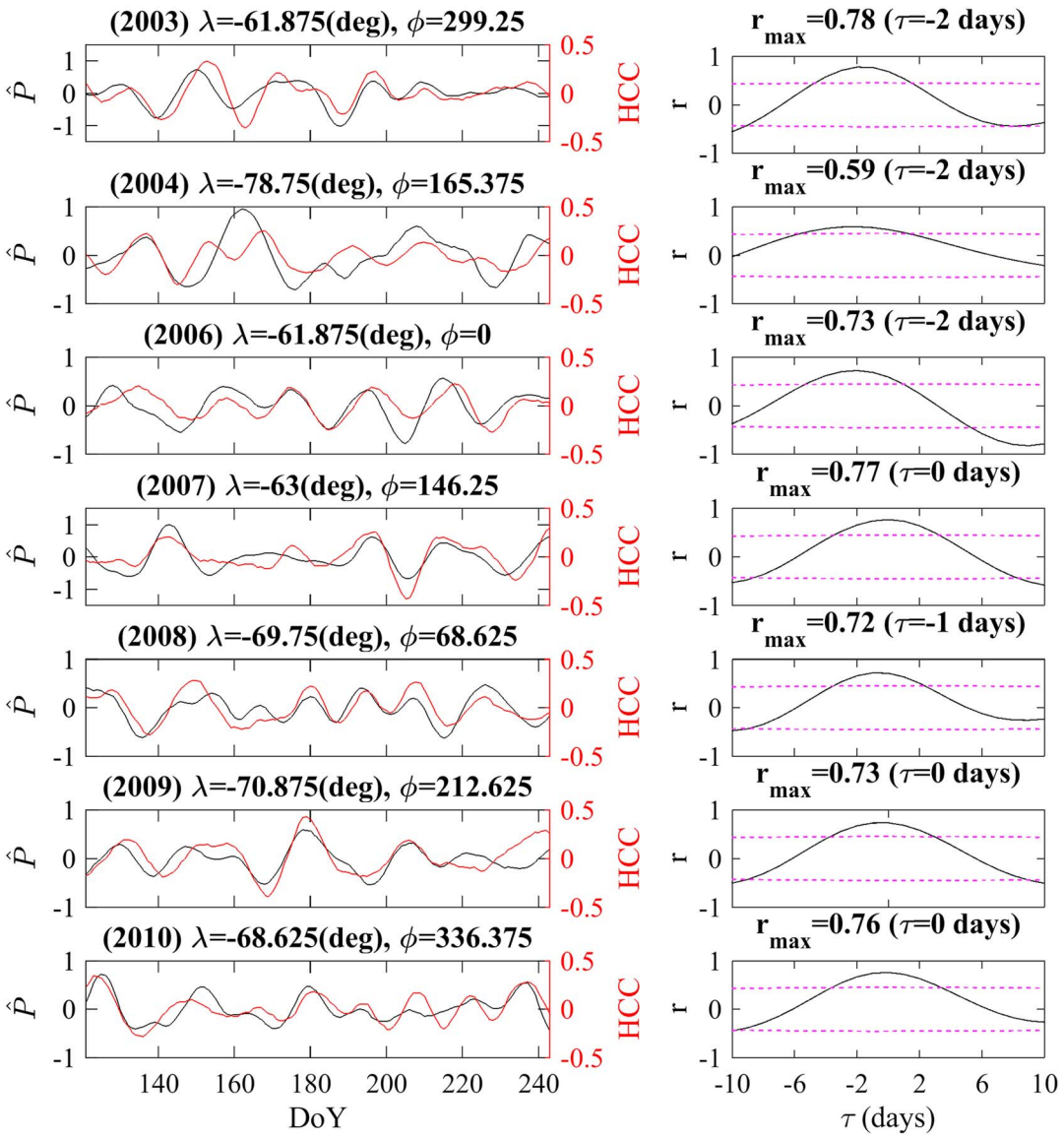

Figure 6. (left column) Examples of $\hat{P}$ and HCC fluctuations, observed during winter months of 2003–2010 years. The time series are band-pass filtered around the ~27 day periodicity. The geographic coordinates of the region corresponding to the HCC filtered time series are indicated. (right column) Cross-correlation analysis as a function of the delay of the HCC with respect to $\hat{P}$, together with the 95% confidence level (magenta lines). A delay $\tau < 0$ ($\tau > 0$) indicates that $\hat{P}$ precedes (follows) HCC.

Regarding C_Q, significantly high variations are found during B_z <0 and B_y >0 conditions, with positive variations in the same polar regions of the observed C_T, while during B_z <0 and B_y <0 conditions, significantly high enhancements are found at lower tropospheric heights and lower latitudes.

Less clear results are observed during $B_z > 0$, for both $B_y < 0$ and $B_y > 0$ conditions.

The above, almost similar, variations of T and Q for different IMF conditions suggest of a possible physical link with the magnetospheric dynamics that manifests during periods characterized by relevant reconnection processes between the IMF and the magnetospheric field.

3.3. Correlation Analysis

We analyzed the correlation between Pc1-2 power and fluctuations of the atmospheric parameters. It is a matter of facts that high coherence values between temperature and ULF power fluctuations have been found, at tropospheric and stratospheric heights, during 2007 by *Regi et al.* [2016], with the clearest correspondence

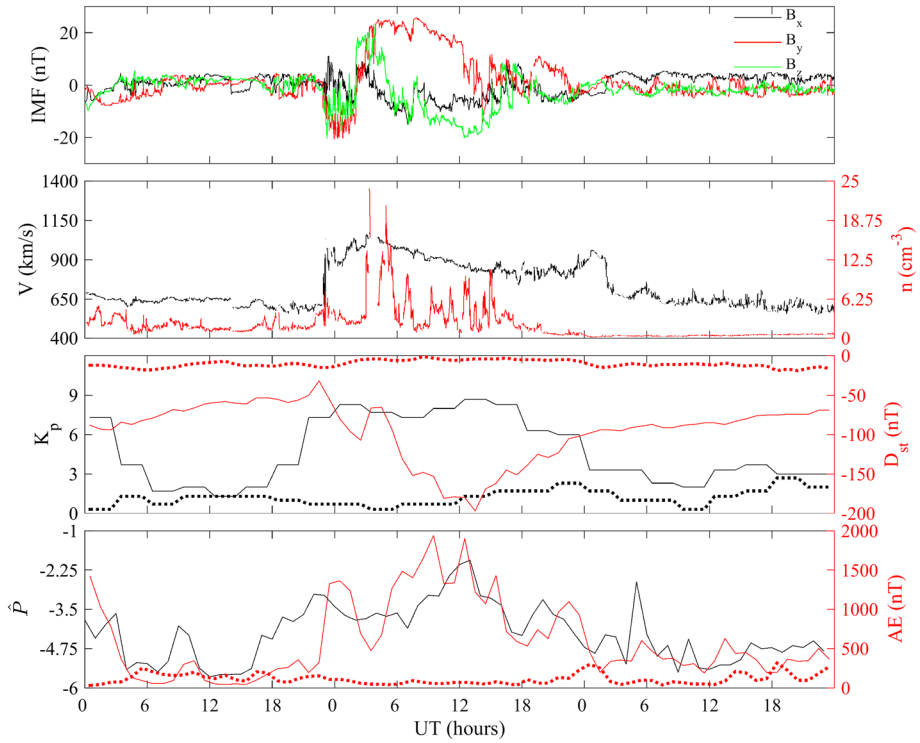

Figure 7. The disturbed geomagnetic periods during 26–28 July 2004. (first to fourth panels) Interplanetary magnetic field in GSE coordinate system; solar wind speed *V* and plasma density *n*; 3 h activity index *Kp* and hourly *Dst*; and hourly auroral activity index *AE* and $\hat{P}$ at Terra Nova Bay. In Figure 7 (third and fourth panels), the quiet time values of the activity indexes (25–27 August) are showed (dotted lines).

at the 27 day periodicity. Following their results, and also on the basis of Figure 1, the time series were filtered in the 20–30 day periodicity range before correlation analysis. Figure 5 shows, for different years, the latitudinal and longitudinal distribution of the correlation between $\hat{P}$ and tropospheric parameters.

For each year, there are several regions characterized by significantly correlated (or anticorrelated) 27 day fluctuations, with a remarkable correspondence in all atmospheric parameters (less clear in LCC). Note that the correlation coefficients of $\hat{P}$ with *T* and *Q* are averaged over the different tropospheric heights, while the correlation coefficients with HCC, MCC, and LCC refer to a single tropospheric layer.

The generally lower correlation with LCC could indicate that the major effect in cloud microphysics manifests at higher altitudes, just below the tropopause. It is also evident that correlated/anticorrelated fluctuations appear in well-defined regions but different for different years. A possible relationship with large-scale atmospheric transport was investigated by means of a correlation analysis between $\hat{P}$ and CH_4 (20–30 day filtered) concentrations from MACC data set. CH_4 is a long life chemical tracer, commonly used to characterize the middle atmosphere transport, also analyzing it in the framework of quasi-Lagrangian or conservative coordinate systems [see, e.g., *Redaelli et al.*, 1994] and as a proxy to validate satellite measurements [e.g., *Payan et al.*, 2009]. The results of the correlation analysis between $\hat{P}$ and CH_4, during 2003–2010 (not shown here), indicate that the correlation coefficients are generally lower and not superimposable to the other tropospheric parameters. These results suggest that the transport is not modulated by the 27 day periodicity of the ULF activity. However, the different pattern for various years could be due to variations in large-scale transport pattern.

To estimate the time delay between the ULF power and the atmospheric parameters, from the correlation maps shown in Figure 5, we selected, for each year, the region with the highest correlation values between ULF power and HCC fluctuations (Figure 6, left column). For each year we estimated the delay, computing the cross-correlation coefficient *r* as a function of the time delay τ (Figure 6, right column). Here a negative (positive) τ, associated with the maximum correlation, indicates that the ULF power fluctuations precede

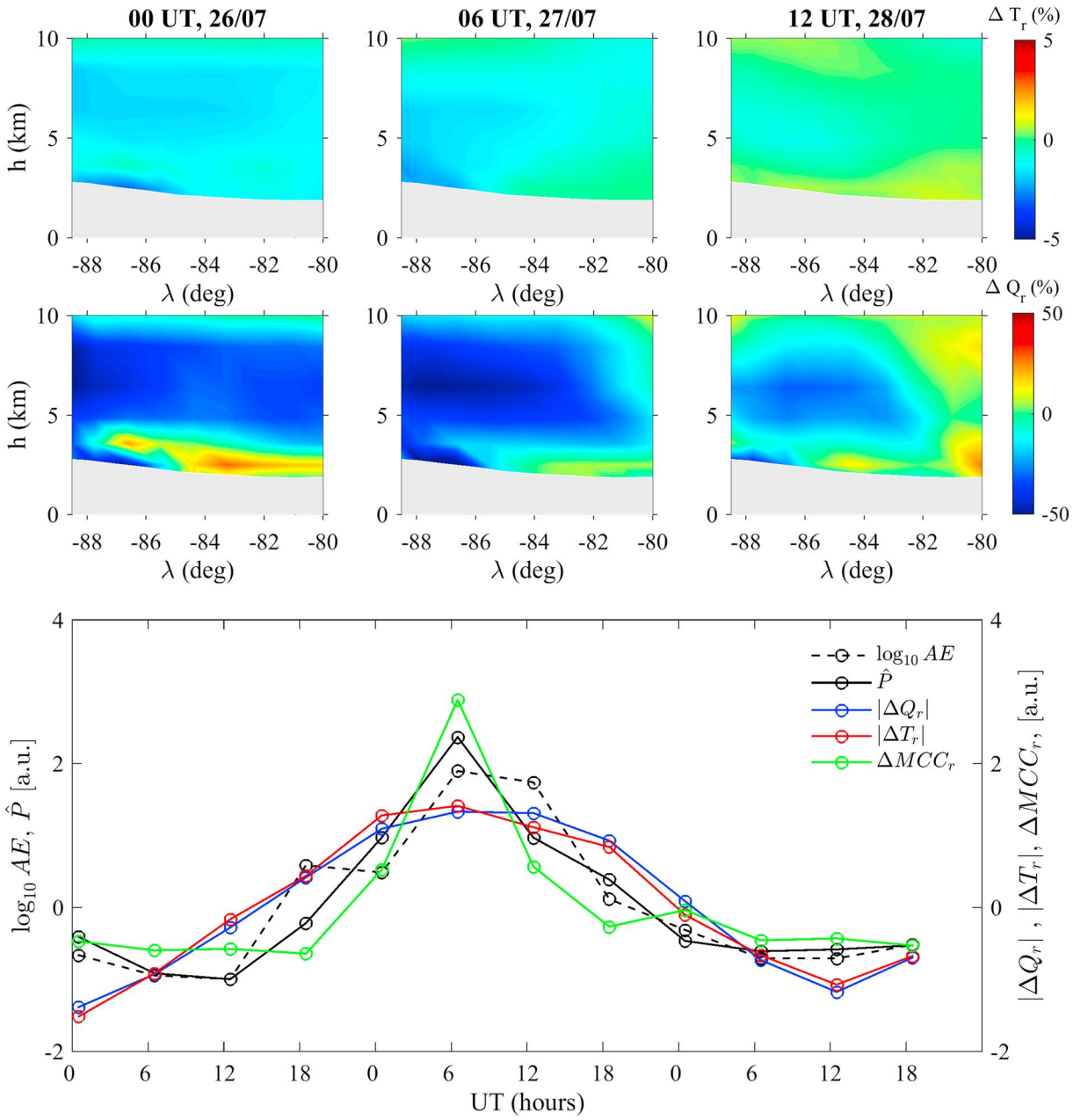

Figure 8. (top) Time evolution of tropospheric zonal mean temperature and specific humidity with respect to quiet geomagnetic period, at selected time intervals on 26–28 July 2004. (bottom) The comparison between averaged of detrended atmospheric parameters ΔT_r, ΔQ_r, and $\Delta \mathrm{MCC}_r$, with the auroral activity *AE* and $\hat{P}$ at TNB. The average was computed for $3 < h < 8$ km and in the latitudinal range 80–89°S.

(follow) the HCC ones. It clearly emerges that the highest correlations (outside the 95% confidence level, Figure 6, magenta lines) were found when the ULF activity precedes the HCC, by 0–2 days, consistent with both the SEA analysis and the ground temperature behavior found by *Francia et al.* [2015].

4. Atmospheric Response During Polar Geomagnetic Storms

In order to further investigate the short time tropospheric response to geomagnetic activity, we used 6 h reanalysis data set. We selected periods characterized by high pulsation activity (high $\hat{P}$).

In order to study the response of each atmospheric parameter to the geomagnetic activity, we compared their variations during the geomagnetically disturbed time interval and the nearest (within 1 month) quiet

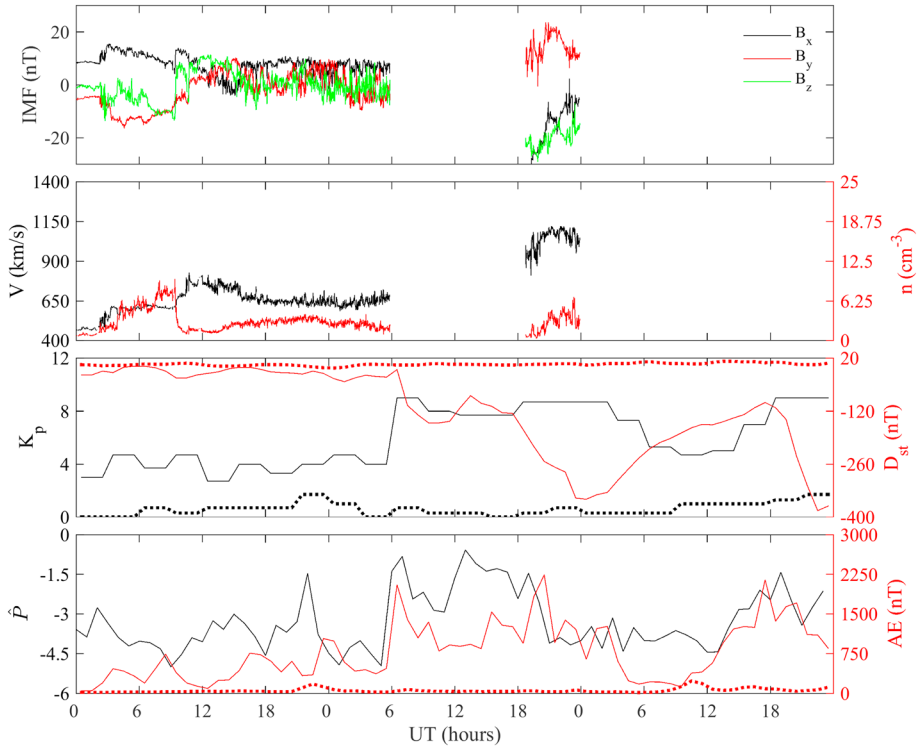

Figure 9. The disturbed geomagnetic periods during 28–30 October 2003. (first to fourth panels): Interplanetary magnetic field in GSE coordinate system; solar wind speed *V* and plasma density *n*; 3 h activity index *Kp* and hourly *Dst*; and hourly auroral activity index *AE* and $\hat{P}$ at Terra Nova Bay. In Figure 9 (third and fourth panels), the quiet time values of the activity indexes (10–12 October) are showed (dotted lines).

geomagnetic period. We computed the relative variations of the zonal mean temperature T_z, specific humidity Q_z, and cloud cover CC_z, as

$$\Delta X_r = \left(X_{z,d} - X_{z,q}\right) / X_{z,q} \tag{1}$$

where *d* and *q* indicate "disturbed" and "quiet" geomagnetic activity conditions, respectively. We removed from each zonal mean the linear trend in the examined time range (accordingly with SEA procedure). Finally, 1 h Pc1-2 and *AE* data were resampled at 6 h time resolution, using decimation procedure, in order to compare their variations with those of the atmospheric parameters.

4.1. Polar Storm On 27 July 2004

Figure 7 shows the event on 26–28 July 2004. The geomagnetic storm occurred on 27 July when the interplanetary magnetic field component B_z was negative during the intervals ~0–3 UT and ~6–18 UT, while the solar wind speed *V* and plasma density *n* were high during the whole day. Both *AE* and $\hat{P}$ activity indexes clearly indicate a disturbed magnetosphere. This event follows the geomagnetic storm on 24 July 2004, classified as positive geomagnetic storm [*Ngwira et al.*, 2012; *Suvorova et al.*, 2012], i.e., characterized by an increase in the ionospheric electron density at middle and low-latitude ionosphere. As representative of the nearest quiet geomagnetic conditions we selected the time interval 25–27 August 2004 (the corresponding *AE*, *Kp*, and *Dst* are shown by dotted lines).

In Figure 8 (top) the relative variations of *T*, *Q*, MCC, $\hat{P}$, and $\log_{10}$ *AE* (we used $\log_{10}$ *AE* instead of *AE*, as for the Pc1-2 power) are compared at different times. It can be seen that ΔQ_r is negative with minimum values on 27 July at medium/high tropospheric heights, while it is positive from ground up to 3–4 km, i.e., at the typical altitudes of low-altitude clouds and up to about 80°S suggesting that geomagnetic activity might principally act by modulating scavenging processes in clouds. A less clear trend is found in ΔT_r.

We computed the average of the relative variations in each parameter in the examined spatial range of 3–8 km and 80–89°S, as a function of time, and reported the results in Figure 8 (bottom). A clear relationship was found during this period, when both geomagnetic and atmospheric variations are almost simultaneous,

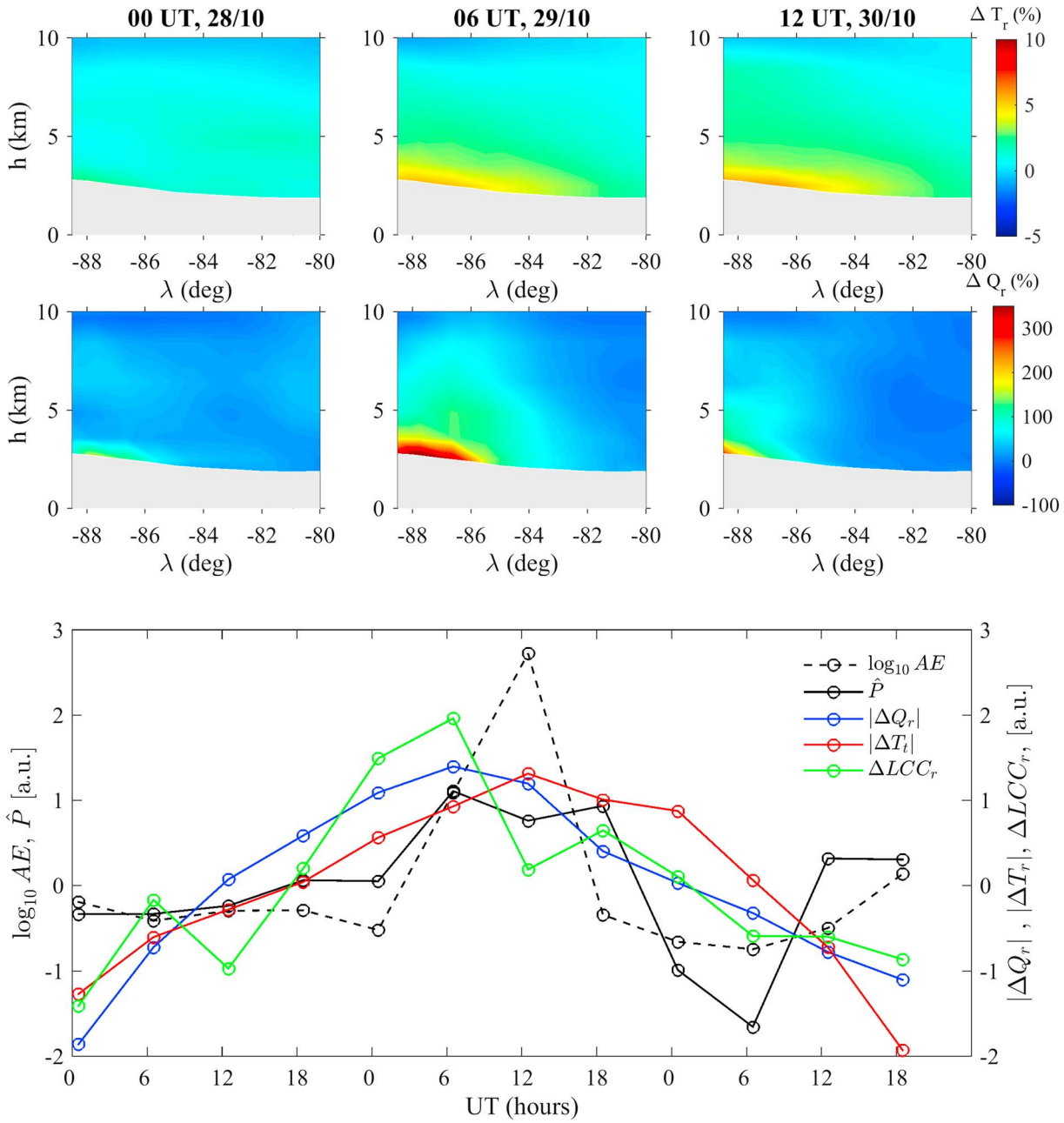

Figure 10. (top) Time evolution of tropospheric zonal mean temperature and specific humidity with respect to quiet geomagnetic period, at selected time intervals on 28–30 October 2003. (bottom) The comparison between averaged of detrended atmospheric parameters ΔT_r, ΔQ_r, and ΔLCC_r, with the auroral activity *AE* and $\hat{P}$ at TNB. The average was computed for $3 < h < 8$ km and in the latitudinal range 80–89°S.

within 6 h. In particular, the best correspondence was found between *AE* or $\hat{P}$ with medium cloud cover relative variations ΔMCC.

4.2. Polar Storm on 29 October 2003

We selected the equinoctial geomagnetic storm occurring on 29 October 2003, also known as Halloween Super Storm [*Villante and Regi*, 2008; *Tsurutani*, 2005], recently classified as a Carrington-like geomagnetic storm [*Cid et al.*, 2014; *Saiz et al.*, 2016]. It was generated by the magnetospheric response to the impacting plasma cloud ejected in the interplanetary space, after a X17 solar flare on 28 October 2003 [*Villante and Regi*, 2008]. In particular, in the extreme ultraviolet band, this event was by far the largest one in the active period October–November 2003 [*Tsurutani*, 2005].

Figure 9 shows the interplanetary conditions during 28–30 October 2003, as well as the geomagnetic activity indexes. As representative of the nearest quiet geomagnetic conditions we selected the time interval 10–12 October 2003 (the corresponding *AE*, *Kp*, and *Dst* are shown by dotted lines). In this case, we found an increase of auroral and ULF activity starting from ~6 UT ($Kp \sim 10$, $AE \sim 1900$ nT) on 29 October and ending at ~6 UT on 30 October. During this long-lasting geomagnetic activity the atmospheric parameter response reveals increasingly strong positive variations in ΔT_r and ΔQ_r, at $h \sim 3.5$ km (close to the ground) and $\lambda \sim 88°$S (Figure 10).

We also examined the relative variation of cloud cover during the same time interval, and we found that the major effect of Pc1-2 power fluctuations is observed in the low-altitude cloud cover, with respect to the other cloud covers. In particular, Δ LCC$_r$ reflects the same time dependence of ΔQ_r, with the largest value at ~06 UT on 29 October, i.e., when $\hat{P}$ reaches its first maximum value.

5. Discussions and Conclusions

We investigated the atmospheric response to geomagnetic activity in Antarctica using the Pc1-2 power fluctuations at TNB, during the 2003–2010 years. The wavelet analysis conducted during the minimum phase of the solar cycle 23 clearly shows the signatures of the 27 day ULF activity main periodicity (and its subharmonics) in the tropospheric temperature and specific humidity provided by MACC assimilated atmospheric model: this result confirms the conclusions by *Francia et al.* [2015] and *Regi et al.* [2016]; it is probably due to stable low-latitude coronal holes responsible for recurrent solar wind structures observed around the minimum phase of solar cycle.

The results obtained by means of SEA analysis and correlation/cross-correlation analyses revealed a clear correspondence between Pc1-2 variations and variations in temperature, specific humidity, and cloud cover reanalysis data set. The most significant correspondence was found at latitudes higher than 85°S in all parameters within 2 days of the maximum geomagnetic activity at TNB, in particular in correspondence to the IMF conditions $B_z < 0$ and $B_y > 0$; it suggests that during periods characterized by reconnected magnetosphere and strong south-north interplanetary electric field, the atmospheric response is high. Assuming a radial solar wind speed $\mathbf{V} \sim -V\hat{x}$ (where $\hat{x}$ is the Sun-Earth line, and $V(>0)$ is the solar wind speed), the interplanetary electric field (IEF), $\mathbf{E} = -\mathbf{V} \times \mathbf{B} \sim \left(-VB_z\right)\hat{y} + \left(VB_y\right)\hat{z}$, lies in the *y*-*z* plane in the GSM reference system. During $B_z < 0$ conditions, the IEF is efficiently transmitted over the high-latitude ionosphere, and the dawn-dusk polar cap potential difference Φ_{cap}, due to $E_y = -VB_z$, as well as the vertical $E_z = VB_y$, increase. These results are in agreement with *Voiculescu et al.* [2013], who found a significant positive correlation between LCC and a positive E_y component of the IEF (corresponding to a negative B_z), especially at high latitudes. We found, in a separated analysis not shown here, that the correlation between E_y and HCC band-pass filtered data (~27 days) was high, showing the same patterns of the correlation maps shown in Figure 5.

We found that the correspondence between band-pass filtered (~27 days) tropospheric and geomagnetic parameters is an average of correlated and anticorrelated regions. In particular, during each year, the correlation (and anticorrelation) maps the same regions, for all atmospheric parameters, with maximum values obtained for the high-altitude cloud cover.

Moreover, examining the correlation at different time delays, we found that the maximum values were found within 0–2 days with respect to the geomagnetic activity variations, consistently with *Francia et al.* [2015], who investigated the surface air temperature response to ULF geomagnetic activity and found a $\tau \sim 1$ and 2 days with Pc1-2 and Pc5 power fluctuations, respectively.

Because the atmospheric parameters seem to respond quickly to geomagnetic activity variations, we further investigated the tropospheric-geomagnetic relationship in the polar cap, using the 6 h reanalysis data set. We focused on two strong geomagnetic storms that occurred on 27–29 July 2004 and on 29–30 October 2003. Both storms evidenced high relative variations of temperature, specific humidity, and cloud cover within 6 h but at different latitudes, with clear variation in the specific humidity, at tropospheric heights and in correspondence of maximum polar cap activity, accordingly with SEA results.

The present experimental results, obtained over a more extended time interval and for different parameters, confirm the suggestion by *Francia et al.* [2015] and *Regi et al.* [2016], i.e., a possible effect of both ionization and

polar cap potential variations on high-latitude atmospheric conditions, within 1–2 days, particularly evident at the 27 day periodicity related to solar wind/geomagnetic variations.

The results indicate that the solar wind energy is efficiently transferred to polar tropospheric regions, during periods characterized by $B_z < 0$, affecting the polar cap potential Φ_{cap}; moreover, the increasing precipitation rate of the relativistic electrons, related with increasing ULF activity in the Pc1-2 frequency range, modifies the atmosphere conductivity. Both mechanisms could affect atmospheric parameters by modulating microphysical processes in the clouds, through changes in scavenging rates, leading to changes in cloud properties and in the amount of water vapor and latent heat released during evaporation/condensation cycles.

Acknowledgments
This research activity was supported by the Italian PNRA (Programma Nazionale di Ricerche in Antartide, PdR2013/B2.09). The authors acknowledge J.H. King and N. Papatashvilli at NASA and CDAWeb for solar wind data (http://cdaweb.gsfc.nasa.gov). Authors would also like to thank the ECMWF/MACC project data provider. The MACC reanalysis data can be downloaded from the ECMWF Data Server (http://apps.ecmwf.int/datasets/data/macc_reanalysis/). Measurements of the magnetic field fluctuations at Terra Nova Bay can be requested to Marcello De Lauretis at the following e-mail address: marcello.delauretis@aquila.infn.it.

References

Arnoldy, R., et al. (2005), Pc 1 waves and associated unstable distributions of magnetospheric protons observed during a solar wind pressure pulse, *J. Geophys. Res.*, *110*, A07229, doi:10.1029/2005JA011041.

Baumgaertner, A. J., A. Seppälä, P. Jöckel, and M. A. Clilverd (2011), Geomagnetic activity related NOx enhancements and polar surface air temperature variability in a chemistry climate model: Modulation of the NAM index, *Atmos. Chem. Phys.*, *11*(9), 4521–4531.

Blum, L., et al. (2015), Observations of coincident EMIC wave activity and duskside energetic electron precipitation on 18–19 January 2013, *Geophys. Res. Lett.*, *42*, 5727–5735, doi:10.1002/2015GL065245.

Chree, C. (1913), Some phenomena of sunspots and of terrestrial magnetism at Kew observatory, *Philos. Trans. R. Soc. A*, *212*, 75–116, doi:10.1098/rsta.1913.0003.

Cid, C., J. Palacios, E. Saiz, A. Guerrero, and Y. Cerrato (2014), On extreme geomagnetic storms, *J. Space Weather Space Clim.*, *4*, A28, doi:10.1051/swsc/2014026.

De Lauretis, M., P. Francia, M. Regi, U. Villante, and A. Piancatelli (2010), Pc3 pulsations in the polar cap and at low latitude, *J. Geophys. Res.*, *115*, A11223, doi:10.1029/2010JA015967.

de Wit, T. D., and J. Watermann (2010), Solar forcing of the terrestrial atmosphere, *C. R. Geosci.*, *342*(4), 259–272, doi:10.1016/j.crte.2009.06.001.

Dyrud, L., M. Engebretson, J. Posch, W. Hughes, H. Fukunishi, R. Arnoldy, P. Newell, and R. Horne (1997), Ground observations and possible source regions of two types of Pc 1-2 micropulsations at very high latitudes, *J. Geophys. Res.*, *102*(A12), 27,011–27,027, doi:10.1029/97JA02191.

Engebretson, M., et al. (2008), Pc1–Pc2 waves and energetic particle precipitation during and after magnetic storms: Superposed epoch analysis and case studies, *J. Geophys. Res.*, *113*, A01211, doi:10.1029/2007JA012362.

Forbush, S., M. Pomerantz, S. Duggal, and C. Tsao (1983), Statistical considerations in the analysis of solar oscillation data by the superposed epoch method, in *Problems of Solar and Stellar Oscillations*, edited by D. O. Gough, pp. 113–122, Springer, Netherlands, doi:10.1007/bf00145551.

Francia, P., M. de Lauretis, M. Vellante, U. Villante, and A. Piancatelli (2009), ULF geomagnetic pulsations at different latitudes in Antarctica, *Ann. Geophys.*, *27*, 3621–3629, doi:10.5194/angeo-27-3621-2009.

Francia, P., M. Regi, and M. De Lauretis (2015), Signatures of the ULF geomagnetic activity in the surface air temperature in Antarctica, *J. Geophys. Res. Space Physics*, *120*, 2452–2459, doi:10.1002/2015JA021011.

Inness, A., et al. (2013), The MACC reanalysis: An 8 yr data set of atmospheric composition, *Atmos. Chem. Phys.*, *13*, 4073–4109, doi:10.5194/acp-13-4073-2013.

Laken, B. A., and J. Čalogović (2013), Composite analysis with Monte Carlo methods: An example with cosmic rays and clouds, *J. Space Weather Space Clim.*, *3*, A29, doi:10.1051/swsc/2013051.

Lam, M. M., and B. A. Tinsley (2016), Solar wind-atmospheric electricity-cloud microphysics connections to weather and climate, *J. Atmos. Sol. Terr. Phys.*, *149*, 277–290, doi:10.1016/j.jastp.2015.10.019.

Lu, H., M. A. Clilverd, A. Seppälä, and L. L. Hood (2008), Geomagnetic perturbations on stratospheric circulation in late winter and spring, *J. Geophys. Res.*, *113*, D16106, doi:10.1029/2007JD008915.

Mann, I., T. O'Brien, and D. Milling (2004), Correlations between ULF wave power, solar wind speed, and relativistic electron flux in the magnetosphere: Solar cycle dependence, *J. Atmos. Sol. Terr. Phys.*, *66*(2), 187–198, doi:10.1016/j.jastp.2003.10.002.

Mironova, I. A., K. L. Aplin, F. Arnold, G. A. Bazilevskaya, R. G. Harrison, A. A. Krivolutsky, K. A. Nicoll, E. V. Rozanov, E. Turunen, and I. G. Usoskin (2015), Energetic particle influence on the Earth's atmosphere, *Space Sci. Rev.*, *194*(1–4), 1–96, doi:10.1007/s11214-015-0185-4.

Mursula, K., L. Blomberg, P.-A. Lindqvist, G. Marklund, T. Bräysy, R. Rasinkangas, and P. Tanskanen (1994), Dispersive Pc1 bursts observed by FREJA, *Geophys. Res. Lett.*, *21*(17), 1851–1854, doi:10.1029/94GL01584.

Ngwira, C. M., L.-A. McKinnell, P. J. Cilliers, and A. J. Coster (2012), Ionospheric observations during the geomagnetic storm events on 24–27 July 2004: Long-duration positive storm effects, *J. Geophys. Res.*, *117*, A00L02, doi:10.1029/2011JA016990.

Payan, S., et al. (2009), Validation of version-4.61 methane and nitrous oxide observed by MIPAS, *Atmos. Chem. Phys.*, *9*(2), 413–442, doi:10.5194/acp-9-413-2009.

Redaelli, G., et al. (1994), UARS MLS O3 soundings compared with lidar measurements using the conservative coordinates reconstruction technique, *Geophys. Res. Lett.*, *21*, 1535–1538, doi:10.1029/94GL00629.

Regi, M., M. De Lauretis, and P. Francia (2015), Pc5 geomagnetic fluctuations in response to solar wind excitation and their relationship with relativistic electron fluxes in the outer radiation belt, *Earth Planets Space*, *67*(1), 9, doi:10.1186/s40623-015-0180-8.

Regi, M., M. De Lauretis, G. Redaelli, and P. Francia (2016), ULF geomagnetic and polar cap potential signatures in the temperature and zonal wind reanalysis data in Antarctica, *J. Geophys. Res. Space Physics*, *121*, 286–295, doi:10.1002/2015JA022104.

Rodger, C. J., T. Raita, M. A. Clilverd, A. Seppälä, S. Dietrich, N. R. Thomson, and T. Ulich (2008), Observations of relativistic electron precipitation from the radiation belts driven by EMIC waves, *Geophys. Res. Lett.*, *35*, L16106, doi:10.1029/2008GL034804.

Rosenfeld, D., U. Lohmann, G. B. Raga, C. D. O'Dowd, M. Kulmala, S. Fuzzi, A. Reissell, and M. O. Andreae (2008), Flood or drought: How do aerosols affect precipitation?, *Science*, *321*(5894), 1309–1313, doi:10.1126/science.1160606.

Rozanov, E., L. Callis, M. Schlesinger, F. Yang, N. Andronova, and V. Zubov (2005), Atmospheric response to NOy source due to energetic electron precipitation, *Geophys. Res. Lett.*, *32*, L14811, doi:10.1029/2005GL023041.

Saiz, E., A. Guerrero, C. Cid, J. Palacios, and Y. Cerrato (2016), Searching for carrington-like events and their signatures and triggers, *J. Space Weather Space Clim.*, *6*, A6, doi:10.1051/swsc/2016001.

Seppälä, A., C. E. Randall, M. A. Clilverd, E. Rozanov, and C. J. Rodger (2009), Geomagnetic activity and polar surface air temperature variability, *J. Geophys. Res.*, *114*, A10312, doi:10.1029/2008JA014029.
Seppälä, A., H. Lu, M. A. Clilverd, and C. J. Rodger (2013), Geomagnetic activity signatures in wintertime stratosphere wind, temperature, and wave response, *J. Geophys. Res. Atmos.*, *118*, 2169–2183, doi:10.1002/jgrd.50236.
Suvorova, A., L. Tsai, and A. Dmitriev (2012), On magnetospheric source for positive ionospheric storms, *Sun Geosphere*, *7*(2), 91–96.
Tinsley, B. A., and R. A. Heelis (1993), Correlations of atmospheric dynamics with solar activity evidence for a connection via the solar wind, atmospheric electricity, and cloud microphysics, *J. Geophys. Res.*, *98*(D6), 10,375–10,384, doi:10.1029/93JD00627.
Tinsley, B. A., and F. Yu (2004), Atmospheric ionization and clouds as links between solar activity and climate, in *Solar Variability and Its Effects On Climate*, edited by J. M. Pap et al., pp. 321–339, AGU, Washington, D. C., doi:10.1029/141GM22.
Tinsley, B. A., and L. Zhou (2006), Initial results of a global circuit model with variable stratospheric and tropospheric aerosols, *J. Geophys. Res.*, *111*, D16205, doi:10.1029/2005JD006988.
Tinsley, B. A., G. Burns, and L. Zhou (2007), The role of the global electric circuit in solar and internal forcing of clouds and climate, *Adv. Space Res.*, *40*(7), 1126–1139, doi:10.1016/j.asr.2007.01.071.
Torrence, C., and G. P. Compo (1998), A practical guide to wavelet analysis, *Bull. Am. Meteorol. Soc.*, *79*(1), 61–78, doi:10.1175/1520-0477(1998)079<0061:apgtwa>2.0.co;2.
Troshichev, O. A., and A. Janzhura (2004), Temperature alterations on the Antarctic ice sheet initiated by the disturbed solar wind, *J. Atmos. Sol. Terr. Phys.*, *66*(13), 1159–1172, doi:10.1016/j.jastp.2004.05.005.
Tsurutani, B. T. (2005), The October 28, 2003 extreme EUV solar flare and resultant extreme ionospheric effects: Comparison to other Halloween events and the Bastille Day event, *Geophys. Res. Lett.*, *32*, L03S09, doi:10.1029/2004GL021475.
Vellante, M., U. Villante, M. De Lauretis, and P. Cerulli-Irelli (1989), An analysis of micropulsation events at a low-latitude station during 1985, *Planet. Space Sci.*, *37*(7), 767–773, doi:10.1016/0032-0633(89)90128-1.
Villante, U., and M. Regi (2008), Solar flare effect preceding Halloween storm (28 October 2003): Results of a worldwide analysis, *J. Geophys. Res.*, *113*, A00A05, doi:10.1029/2008JA013132.
Voiculescu, M., I. Usoskin, and S. Condurache-Bota (2013), Clouds blown by the solar wind, *Environ. Res. Lett.*, *8*(4), 045032, doi:10.1088/1748-9326/8/4/045032.
Wallace, J. M., and P. V. Hobbs (2011), *Atmospheric Science*, Elsevier Acad. Press, Amsterdam.
Yagova, N., L. Lanzerotti, U. Villante, V. Pilipenko, S. Lepidi, P. Francia, V. Papitashvili, and A. Rodger (2002), ULF Pc5-6 magnetic activity in the polar cap as observed along a geomagnetic meridian in Antarctica, *J. Geophys. Res.*, *107*(A8), 1195, doi:10.1029/2001JA900143.